Macromolecules

ARTICLE

pubs.acs.org/Macromolecules

Low Bandgap Polymers Based on Regioregular Oligothiophenes Linked with Electron Accepting Units

Luozheng Zhang,[†] Keisuke Tajima,*[,†,‡] and Kazuhito Hashimoto*[,†,‡]

[†]Department of Applied Chemistry, School of Engineering, The University of Tokyo, 7-3-1 Hongo, Bunkyo-ku, Tokyo 113-8656, Japan

[‡]HASHIMOTO Light Energy Conversion Project, ERATO, Japan Science and Technology Agency (JST)

Supporting Information

ABSTRACT:

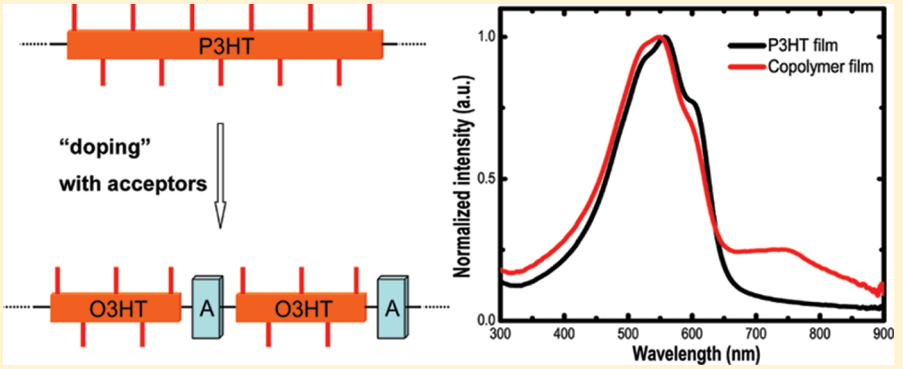

A synthetic route was developed to introduce an electron accepting unit, 2,5-di(2-ethylhexyl)pyrrolo[3,4-*c*]pyrrole-1,4-dione (DPP), into the main chain of regioregular poly(3-hexylthiophene) (P3HT) at a low concentration (ca. 4.5 mol % in monomer ratio), in order to lower the optical bandgap and simultaneously retain high hole mobility in P3HT. First, regioregular oligo(3-hexylthiophene) (O3HT), a macromonomer with a narrow polydispersity, was synthesized by Ni-catalyzed Grignard metathesis polymerization and subsequent stannylation of the chain ends. The copolymer was then synthesized by Stille coupling between the DPP unit and the macromonomer. The copolymer exhibits an extended absorption shoulder up to 750 nm, in addition to the original absorption of P3HT, as a result of intramolecular charge transfer. X-ray diffraction, field-effect transistor measurements, and UV−vis absorption of the polymer films showed that the crystal structure and high hole mobility were retained, owing to the regioregular O3HT blocks. Organic solar cells based on the copolymer and [6,6]-phenyl-C_{61}-butyric acid methyl ester showed a broad photocurrent response of up to 900 nm and a power conversion efficiency of 2.07% without deterioration of the fill factor.

INTRODUCTION

Extensive research has been conducted on organic solar cells (OSCs) because they are lightweight, are inexpensive to produce, and can potentially be used in flexible devices. OSCs based on a typical donor of regioregular poly(3-hexylthiophene) (P3HT) and acceptor of [6,6]-phenyl-C_{61}-butyric acid methyl ester (PCBM) have been reported to achieve a power conversion efficiency (PCE) of up to 4.5% with the structure of so-called bulk heterojunction.[1] It has been confirmed that the high regioregularity of P3HT is an important factor in high PCE, since it leads to high crystallinity of the polymer and the formation of hole-conducting interpenetrating paths in the bulk heterojunction.[2,3] To further improve PCE, a promising approach is to employ semiconducting polymers with a broader, stronger absorption. A common strategy relies on donor−acceptor (D−A) alternating copolymers, where the backbone is composed of an electron-rich donor unit and an electron-deficient acceptor unit. These polymers could show intramolecular charge transfer (ICT) from the donor to the acceptor unit upon photoexcitation, resulting in a lower bandgap and consequently a lower energy absorption band. Several OSCs based on these types of polymers have recently been reported to show PCEs of over 6%.[4−7] However, there are several drawbacks to the design principles of D−A alternating copolymers. Although ICT shifts the absorption band to the longer wavelength region, the absorbance in the short wavelength range is generally weakened or even lost, owing to the large splitting of the absorption band.[8−11] Moreover, D−A alternating copolymers with acceptor units having strong electron affinity in the backbone often show lower charge carrier mobility compared with highly crystalline semiconducting polymers, possibly due to the localized highest occupied molecular orbital (HOMO) in the main chain, or less ordered interchain packing induced by the lower regularity of the polymer structures.[2,11]

Received: February 8, 2011
Revised: April 25, 2011
Published: May 06, 2011

In this paper, we propose a new approach to designing a low bandgap (LBG) polymer with broad light absorption and high hole mobility, by doping the main chain of a highly crystalline semiconducting polymer with a small amount of the acceptor unit. To demonstrate this, we selected P3HT for the parent structure because of its high crystallinity and high hole mobility. The oligo(3-hexylthiophene) (O3HT) (oligomer **1** in Scheme 1) was first synthesized through the Ni-catalyzed chain growth polymerization method reported previously,[12,13] and then a new synthetic route to the macromonomer **2** was developed for stannylation of both the chain ends. The copolymer was synthesized by Stille coupling between the 2,5-di(2-ethylhexyl)pyrrolo[3,4-*c*]pyrrole-1,4-dione (DPP) acceptor unit and the macromonomer. The DPP unit has been shown to possess a planar, well-conjugated structure, resulting in a strong $\pi-\pi$ interaction, and the lactam component furnishes a highly electron-withdrawing DPP unit.[9,14] As a result, the DPP unit has been widely exploited in the field of transistors and photovoltaics in the form of both the semiconducting polymers[15,16] and molecular based materials.[17] To enhance the solubility of the copolymer, a 2-ethylhexyl alkyl chain was attached to the DPP unit. The resulting polymer has regioregular O3HT blocks that could induce ordered intermolecular packing and high hole mobility similar to P3HT. The acceptor group in the main chain would give a lower bandgap by ICT, while retaining the original absorption of O3HT.

Although several D−A type copolymers based on alternating copolymerization between oligothiophene blocks and acceptors have been reported for OSC applications,[18−21] there are major differences between past work and the present study. First, the length of the oligothiophene in this study is much larger (degree of polymerization $n \sim 22$) than previously reported (typically $n \sim 2-8$), which should minimize the impact of the introduction of the acceptor unit on the $\pi-\pi$ stacking of P3HT. Second, the regioregularity of the oligothiophene in our design is very high due to the well-controlled Ni-catalyzed oligomerization, which should lead to higher crystallinity. Finally, the current approach should also enable us to rationally tune the optical and electronic properties of the polymers by changing the length of the O3HT blocks (i.e., the doping level of the acceptor units) via a simple change in the monomer/Ni ratio for the oligomerization. This would be difficult in the conventional step-by-step synthesis of the oligomer blocks, especially when the oligothiophene is long.

EXPERIMENTAL SECTION

Syntheses. 3,6-Di(2-bromothien-5-yl)-2,5-di(2-ethylhexyl)pyrrolo[3,4-*c*]pyrrole-1,4-dione (**3**) was synthesized as previously reported.[22] Other chemicals were purchased from Aldrich or Wako Chemicals and used without further purification.

Regioregular Oligo(3-hexylthiophene) (1). Oligomer **1** was synthesized according to the literature, as shown in Scheme 1.[23,24] A 200 mL flask was charged with 2-bromo-3-hexyl-5-iodothiophene (2500 mg, 6.7 mmol) and then evacuated under reduced pressure to remove residual water and oxygen. After the addition of dry THF (67 mL), the solution was cooled to 0 °C in an ice−water bath. A solution of *i*-PrMgCl in THF (2 mol L^{-1}, 3.35 mL) was added dropwise, and the resultant mixture was stirred for 30 min. After the bath was removed, the Ni(dppp)Cl_2 catalyst (181.6 mg, 0.335 mmol) was immediately added to the solution. After 30 min, the reaction was quenched with 5 mol L^{-1} HCl aqueous solution. The organic layer was then extracted with $CHCl_3$, washed three times with $NaHCO_3$(aq) and water, and then dried with $MgSO_4$. After removing the solvent by rotary evaporation, compound **1** was collected by sequential washing with MeOH and hexane. Yield: 64%. Number-averaged molecular weight (M_n): 4990; polydispersity index (PDI): 1.09. ^{1}H NMR (500 MHz, $CDCl_3$): δ 6.98 (s, 1 H), 2.80 (t, 2 H), 1.71 (quint, 2 H), 1.44 (m, 2 H), 1.35 (t, 4 H), 0.92 (t, 3 H).

Bis(trimethylstannyl) Oligo(3-hexylthiophene) (2). Oligomer **1** (528 mg) was dried under vacuum and dissolved in dry THF (132 mL) under N_2. The solution was cooled to −78 °C, and then *N*,*N*,*N*′,*N*′-tetramethylethylenediamine (TMEDA) (1.9 mL, 120 equiv to oligomer **1**) and *s*-BuLi (1.05 mol L^{-1} in cyclohexane/*n*-hexane, 10.1 mL, 100 equiv) were added dropwise via a syringe. After 1 h, Me_3SnCl (1.0 mol L^{-1} in THF, 21.2 mL, 200 equiv) was added in one portion. After additional stirring for 15 min, the reaction mixture was allowed to warm to room temperature. After stirring for another 3 h, the mixture was poured into MeOH. The precipitate was purified by column chromatography over Al_2O_3 with $CHCl_3$ as the eluent. After removing the solvent, compound **2** was collected by precipitation in hexane and filtration. Yield: 70%. ^{1}H NMR (500 MHz, $CDCl_3$): δ 6.98 (s, 1 H), 2.80 (t, 2 H), 1.71 (quint, 2 H), 1.44 (m, 2 H), 1.35 (t, 4 H), 0.92 (t, 3 H), 0.40 (m, 0.5 H).

Copolymer 4. Compounds **2** (127 mg, 0.0254 mmol) and **3** (17.3 mg, 0.0254 mmol) were dissolved in dry toluene (25 mL) in a round-bottom flask. The solution was purged with N_2 for 30 min to remove residual O_2. After adding $Pd(PPh_3)_4$ (3 mg), the suspension was heated at 120 °C for 48 h. The resulting dark green solution was then cooled and poured into MeOH. The precipitate was collected by filtration, dissolved in $CHCl_3$, and purified by passing through a column filled with Al_2O_3, Celite, and silica gel with $CHCl_3$ as the eluent. The pure copolymer was separated from the mixture of starting materials and copolymer by preparative high-performance liquid chromatography (HPLC) using $CHCl_3$ as the eluent. Finally, product **4** was collected by precipitation in hexane and filtration. Yield: 71%. M_n: 16 750; PDI: 1.37. The ^{1}H NMR spectrum is available in Figure S5.

Measurements. ^{1}H NMR spectra in $CDCl_3$ were measured on a JEOL Alpha FT-NMR spectrometer equipped with an Oxford superconducting magnet system (500 MHz). Matrix-assisted laser desorption/ionization time-of-flight mass spectrometry (MALDI-TOF-MS) was carried out in the reflection ion mode on an Applied Biosystems BioSpectrometry Workstation model Voyager DE-STR spectrometer using dithranol as a matrix and $CHCl_3$ as a solvent. Gel permeation chromatography (GPC) was performed at 40 °C using a Shimadzu Prominence system equipped with a UV detector and $CHCl_3$ as the eluent. The $CHCl_3$ solution was passed through a PTFE filter (pore size: 0.2 μm) before sample injection. Differential scanning calorimetry (DSC) analyses of the polymers were recorded under a N_2 atmosphere at a scan rate of 10 °C min^{-1} on a Rigaku DSC 8230 instrument, with Al_2O_3 as the reference. UV−vis spectra were collected on a JACSO V-650 spectrophotometer. Cyclic voltammograms (CVs) were recorded on an HSV-100 (Hokuto Denkou) potentiostat. A Pt plate coated with a thin polymer film was used as the working electrode. A Pt wire and an Ag/Ag^+ (0.01 mol L^{-1} of $AgNO_3$ in acetonitrile) electrode were used as the counter and the reference electrodes (calibrated vs Fc/Fc^+), respectively. X-ray diffraction (XRD) patterns were recorded on a Rigaku SmartLab 2080B202 diffractometer. Atomic force microscopy (AFM) was conducted in tapping mode with a NanoNavi probe station and an S-image unit (SII NanoTechnology Inc., Japan).

Fabrication and Characterization of Field-Effect Transistors. Field-effect transistors (FETs) were fabricated by the contact film transfer (CFT) method, as previously reported by our group,[25] on highly doped n-type (100) Si substrates (<0.02 Ω cm) covered with 300 nm thermally grown SiO_2. An octadecyltrichlorosilane (OTS) self-assembled monolayer (SAM) was formed to modify the surface of SiO_2. The capacitance of the gate dielectric was C_i = 10.7 nF cm^{-2}. The polymers were dissolved in chlorobenzene with a concentration of 5 g L^{-1} and then spin-coated onto PSS-precoated slide glasses without thermal annealing. After the film transfer onto the Si substrates, the films were

Scheme 1. Synthetic Route to Copolymer 4

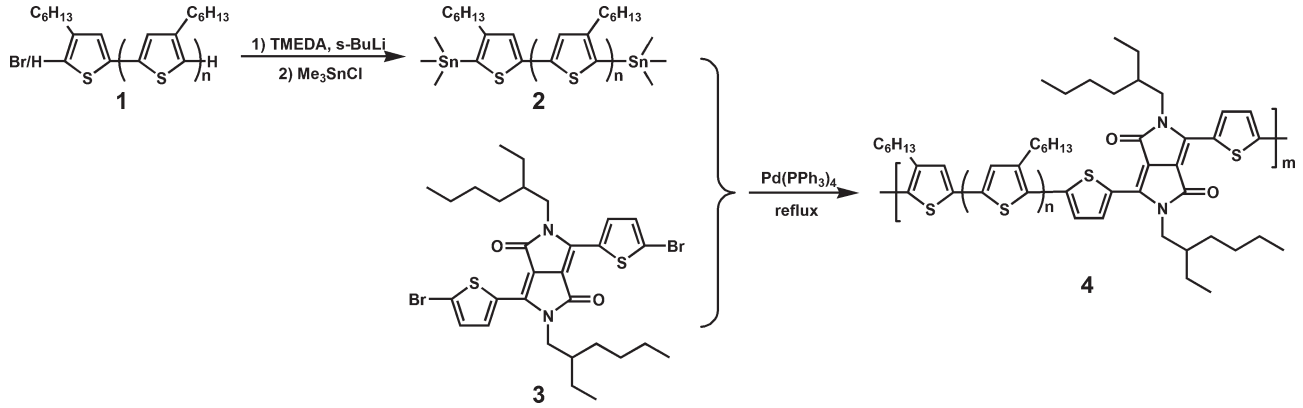

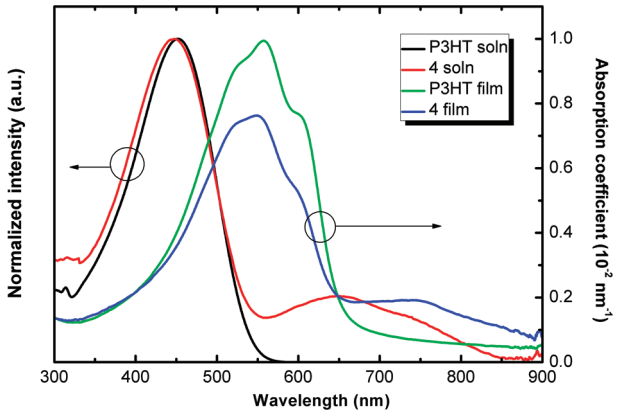

Figure 1. Absorption spectra of P3HT and copolymer **4** in $CHCl_3$ solutions and in spin-coated films from chlorobenzene solutions.

moved into the thermal deposition chamber, where gold electrodes (L = 50 μm and W = 8 mm) were evaporated onto the surface through a metal mask. The electrical characteristics of the transistors were measured with Keithley 2400 and 6430 source/measurement units at room temperature. All the transistors' characteristics were measured in air.

Fabrication and Characterization of Organic Solar Cells. The structure of the OSC was ITO/PEDOT:PSS/copolymer:PCBM/Ca/Al. ITO-coated glass substrates were cleaned by sequential ultrasonication in detergent, deionized water, acetone, and isopropanol. PEDOT:PSS was spin-coated onto the ITO substrate at the rate of 4000 rpm for 30 s. The substrate was transferred into a N_2-filled glovebox, where it was annealed at 150 °C for 5−10 min. After cooling to room temperature, the active layer was spin-coated from a blend solution of donor material and PCBM (donor, 10 g L^{-1}; PCBM, 5−20 g L^{-1}) at a rate of 600−4000 rpm. The substrate was preannealed at 100−180 °C for 5 min before being transferred into the thermal deposition system, where thin layers of Ca (10 nm) and Al (40 nm) were deposited onto the active layer sequentially.

The measurements of photovoltaic performance were conducted under simulated solar light irradiation (AM 1.5, 100 mW cm^{-2}, Peccell Technologies PCE-L11). The irradiated area of the device was defined as 0.06 cm^2 with a photomask. The current−voltage characteristics of the solar cells were measured with the Keithley 2400 I−V measurement system. The light intensity was calibrated with a standard silicon solar cell with an optical filter (Bunkou Keiki BS520). The external quantum efficiency (EQE) of the devices was measured on a Hypermonolight System (Bunkou Keiki SM-250F).

RESULTS AND DISCUSSION

Materials Synthesis. Scheme 1 shows the synthetic route to copolymer **4**. Oligomer **1** was synthesized by Ni-catalyzed polymerization of the monomer 2-bromo-3-hexyl-5-iodothiophene. The monomer/Ni feed ratio was set to 20, while the degree of polymerization determined by ^{1}H NMR was 22.[26] The narrow molecular weight distribution (PDI: 1.09) indicates the living nature of the polymerization.[26] The end groups of oligomer **1** are mainly H-/Br-, confirmed by ^{1}H NMR and MALDI-TOF-MS (Figures S1 and S2) as previously reported.[26,27]

For the synthesis of compound **2**, the end groups of oligomer **1** were lithiated by *s*-BuLi and then stannylated with Me_3SnCl for subsequent Stille coupling. Recently, Lohwasser et al.[28] reported that despite the different properties of the Br- and H- ends, it was possible to functionalize both of the two end groups in P3HT with a carboxyl group. This was done by lithiation of a mixture of P3HT with Br-/H- and H-/H- end groups and subsequent treatment with CO_2. First, we adopted the same strategy as in that report: lithiation with *s*-BuLi for 1 h at −78 °C, deactivation of the residual *s*-BuLi at 40 °C for 20 min, cooling again to −78 °C, and then stannylation with Me_3SnCl. However, we found that this simple treatment of compound **1** did not give distannyl compound **2**. During the lithiation reaction, the reaction mixture at −78 °C exhibited a purple color, indicating that most of the O3HT was aggregated at such a low temperature. This might decrease the reactivity of the end groups on the main chain. TMEDA has been reported to enhance the polarity of alkyllithium species, or break them into smaller clusters, leading to higher reactivity and faster metalation.[29,30] As expected, the addition of TMEDA resulted in the formation of compound **2** (Figure S3). The MALDI-TOF-MS spectrum of **2** in Figure S4 shows that the major end group is the distannyl, and only a minor fraction of Br-/H- was observed. It should be emphasized that this is the first synthesis of O3HT-based stannylated compounds starting from an oligothiophene with more than 20 repeat units and a polydispersive chain length.

Copolymer **4** was synthesized by Stille coupling between macromonomer **2** and **3** and shows high solubility in common organic solvents such as $CHCl_3$, chlorobenzene, and *o*-dichlorobenzene. M_n and PDI of copolymer **4** were 16 750 and 1.37, respectively, as measured by GPC. The M_n is not very high, and this may be due to the small amount of impurities in **2** as suggested by Figure S4, which is known to be effective to reduce the degree of polymerization in condensation polymerizations. The degree

dx.doi.org/10.1021/ma200287a |*Macromolecules* 2011, 44, 4222–4229

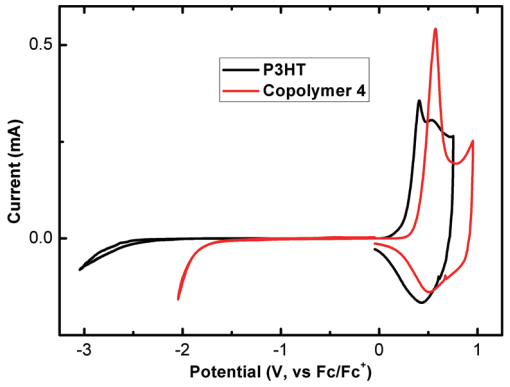

Figure 2. Cyclic voltammogram of P3HT and copolymer **4** films on a platinum plate in an acetonitrile solution of 0.1 mol L^{-1} $[Bu_4N]PF_6$ at a scan rate of 20 mV s^{-1}.

of polymerization in polymer **4**, namely the number *m* in Scheme 1, judging from the M_n of oligomer **1**, is in the range of 3−4.

Optical Properties. The absorption spectra of copolymer **4** are shown in Figure 1. Absorbance of commercial P3HT (Lisicon SP001, Merck Chemicals; M_n = 20 000, PDI = 1.4) is also presented for comparison. In $CHCl_3$ solution, copolymer **4** has two clear absorption bands: one is located in the same region as that of P3HT (350−550 nm), and the other is in the longer wavelength region (550−850 nm) which arises from the ICT between the DPP unit and its adjacent thiophene rings. In comparison to the physical mixture of O3HT and monomer **3** (absorption maximum at 570 nm, see Figure S6), the absorption of DPP moiety in copolymer **4** is significantly red-shifted and broadened. This suggests that the DPP units contribute to the conjugation of the main chain in copolymer **4**. Compared with the peak at ca. 450 nm, the peak at 650 nm possesses much weaker intensity. D−A type alternating copolymers often show a stronger absorption band in longer wavelength than in the shorter wavelength region.[9,10] This difference may reflect the relatively small amount of DPP unit along the main chain in copolymer **4**. Both the absorption peaks shift by about 100 nm in the film state compared with those in solution, suggesting that copolymer **4** has strong intermolecular interactions in the films. A similar band shift between copolymer **4** and P3HT reveals that the incorporated DPP unit does not significantly influence the $\pi-\pi$ stacking in O3HT. The absorption shoulder at around 600 nm, which is generally recognized as an indication of $\pi-\pi$ stacking in P3HT in the solid state,[31] further indicates the high stacking ability of the O3HT blocks in the films of copolymer **4**. Although the absorption coefficient in the film is smaller than that of P3HT in the range of 400−650 nm, copolymer **4** has a broader absorption range. The optical bandgaps of copolymer **4** and P3HT are 1.26 and 1.89 eV, respectively, as estimated from their absorption onsets (980 and 655 nm, respectively), showing that copolymer **4** has a lower bandgap than P3HT.

Electrochemical Properties. To determine the HOMO and lowest unoccupied molecular orbital (LUMO) energy levels of P3HT and copolymer **4**, CV measurement was carried out. Figure 2 shows that the onset values for the oxidation peaks of P3HT and copolymer **4** are +0.27 and +0.41 V vs Fc/Fc^+, respectively; thus, their corresponding HOMO levels are calculated to be −5.07 and −5.21 eV, respectively. The reduction peaks are not reversible, and the reproducibility of the onset potentials was poor. Therefore, the LUMO levels were calculated by adding the optical bandgap to the value of HOMO levels. Using this method, the LUMO levels of P3HT and copolymer **4** are −3.18 and −3.95 eV, respectively. The results indicate that the introduction of the DPP unit into P3HT backbone lowered both the HOMO and LUMO energy levels, but the difference in the LUMO is more significant. This reflects the fact that the electron density of the LUMO is localized at the electron-accepting DPP unit. According to the literature, the LUMO energy levels of copolymer **4** are suitable for the charge separation between PCBM (LUMO level: −4.3 eV).[32]

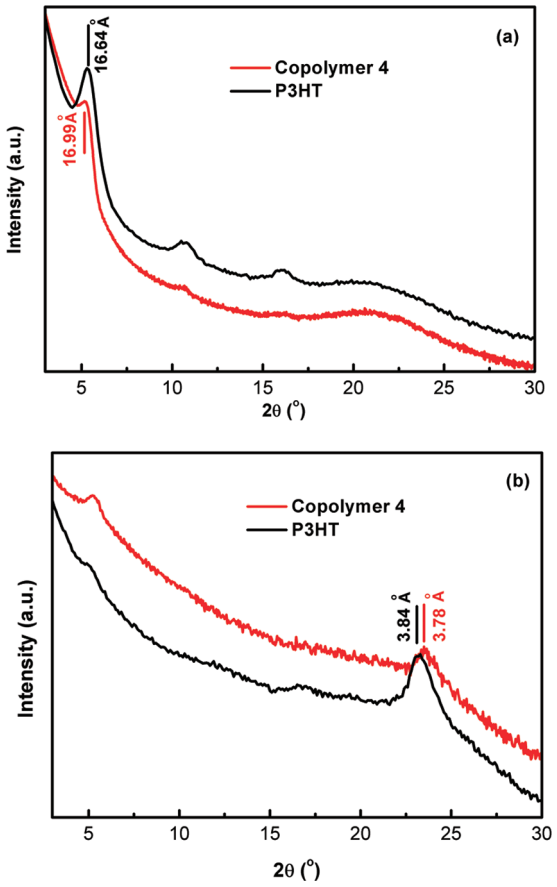

Figure 3. (a) Out-of-plane and (b) in-plane mode XRD patterns of P3HT and copolymer **4** thin films.

X-ray Diffractions of Polymer Films. XRD patterns were measured for the polymer films spin-coated on silicon substrates. Figures 3a and 3b show the patterns with the out-of-plane and in-plane scan modes, respectively. The three peaks at 5.35°, 10.7°, and 16.05° observed in the P3HT film (Figure 3a) can be attributed to a typical lamellar structure with an interlayer distance of 16.64 Å. The copolymer **4** film shows a similar pattern in Figure 3a although the first diffraction peak shows a slightly larger *d*-spacing of 16.99 Å, and the peak intensity is smaller than P3HT. The weaker intensity of those peaks in Figure 3b could indicate a partial edge-on orientation of the lamellar structure in the films. However, the peaks at around 23° in Figure 3b correspond to the intermolecular distances in the direction of $\pi-\pi$ stacking for P3HT and copolymer **4**. The absence of these peaks in the out-of-plane patterns also suggests an edge-on orientation of the lamellar structure. The distances are 3.84 Å for P3HT and 3.78 Å for copolymer **4**. The shorter $\pi-\pi$ stacking distance in copolymer **4** might indicate that the DPP unit in the backbone possesses a stronger stacking

dx.doi.org/10.1021/ma200287a |*Macromolecules* 2011, 44, 4222–4229

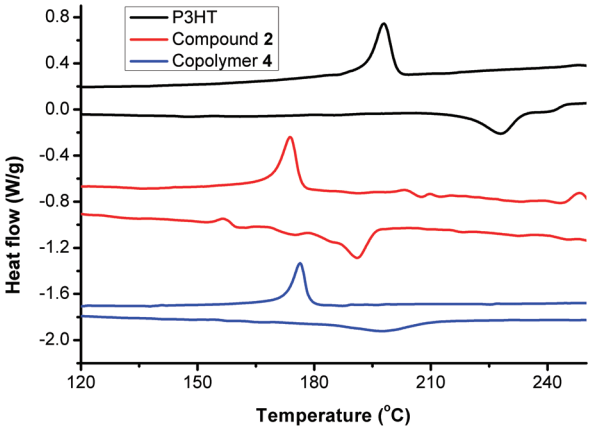

Figure 4. DSC charts of compound **2**, P3HT, and copolymer **4** under a N_2 atmosphere at a scan rate of 10 °C min^{-1}.

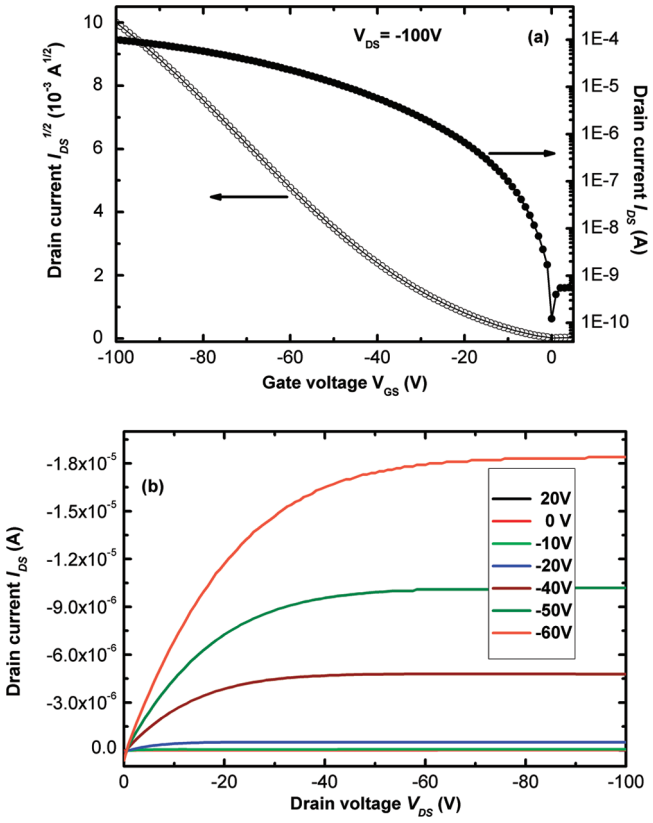

Figure 5. (a) Transfer and (b) output curves of the FET device based on copolymer **4**.

ability and thus that the interaction between adjoining molecules is stronger than in the case of P3HT.

Thermal Characterization. To investigate the influence of doping DPP unit on the crystallinity of the polymers, thermal behaviors of P3HT, compound **2**, and copolymer **4** were analyzed by differential scanning calorimetry (DSC). The third heating and cooling scans are shown in Figure 4 in order to avoid the thermal history. The melting and recrystallization points of P3HT, **2**, and **4** are 228, 191, and 197 °C and 198, 174, and 176 °C, respectively, suggesting that the introduction of DPP units may reduce the size of the crystallized domains in polythiophene.[33]

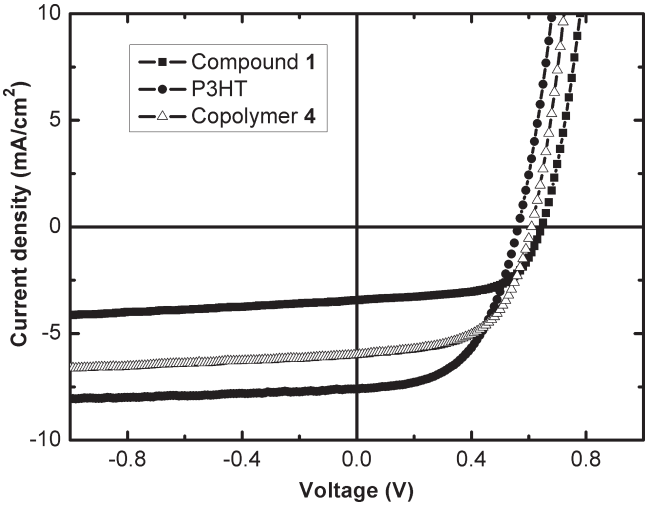

Figure 6. $I-V$ characteristic curves of the photovoltaic devices based on compound **1**, P3HT, and copolymer **4** under the irradiation of AM1.5 (100 mW cm^{-2}).

The enthalpies of fusion of P3HT, **2**, and **4** are about 19, 20, and 14 J g^{-1}, respectively. On the basis of the heat of fusion in the ideal P3HT crystal (99 J g^{-1}),[34] the crystallinities of P3HT, compound **2**, and copolymer **4** are 19%, 20%, and 14%, respectively, implying that the doping of DPP unit into the main chain of P3HT could reduce its crystallinity to a certain extent.

Hole Mobility in Field-Effect Transistors. To check the charge transport property of copolymer **4**, FETs were fabricated using the CFT method developed by our group.[25] Through this method, the polymers investigated showed much higher mobilities in comparison with the conventional methods, owing to the more ordered polymer $\pi-\pi$ stacking structure near the semiconducting polymer/dielectric interface.[25] The transfer curve and output curve are presented in Figure 5. On the basis of the transfer curve measured in the saturation regime ($V_{DS} = -100$ V), the hole mobility of copolymer **4** was estimated to be 0.04–0.06 cm^2 V^{-1} s^{-1}, while the corresponding value for P3HT was 0.16 cm^2 V^{-1} s^{-1}, showing that the charge transport in copolymer **4** is about a quarter of that in P3HT. Previous studies[35] and our recent work on poly(3-alkylthiophene)-based block copolymers[36] both showed that the FETs based on regiorandom P3HT and regioregular poly(3-alkylthiophene) with a branched alkyl chain have a hole mobility of 2–3 orders of magnitude lower than those of regioregular P3HT. Compared with those large impacts of structural disorder on mobility, the introduction of DPP into the P3HT backbone has a less significant effect on the mobility, probably because of the strong interactions of the regioregular O3HT blocks in the polymer.

Photovoltaic Performance. OSCs based on the combination of copolymer **4** and PCBM were fabricated with a bulk heterojunction structure and a typical device configuration. After optimizing the fabrication parameters, it was found that the device showed the highest PCE with a mixed solvent of $CHCl_3$/*o*-dichlorobenzene (volume ratio = 4:1), a blend ratio of 1:0.6 for copolymer **4** to PCBM, and an annealing temperature of 120 °C. For comparison, devices based on compound **1** and P3HT were also fabricated. Their device structures were the same as that of copolymer **4**; however, the solvent was chlorobenzene, and the ratio of the donor to PCBM was 1:0.8. Their $I-V$ curves under AM 1.5 illumination (100 mW cm^{-2}) are presented in Figure 6,

and the photovoltaic characteristics are summarized in Table 1. The performance of the P3HT:PCBM device under the optimized conditions is also included for comparison.

The difference in open-circuit voltage (V_{OC}) between the devices based on P3HT and copolymer **4** can be attributed to the difference in HOMO energy levels observed by CV measurement. However, the higher V_{OC} of compound **1** possibly arises from the less extensive conjugation of the oligomer resulting in a wider bandgap and a deeper HOMO energy level. As shown in Table 1, fill factors (FFs) of the devices are similar in all the polymers, and it is mainly the change in short-circuit current density (J_{SC}) values that causes the difference in PCE.

To investigate the spectral response of the OSCs, external quantum efficiency (EQE) measurements were carried out. As can be seen in Figure 7, the OSC device based on copolymer **4** exhibits an extended response in the long wavelength region up to about 900 nm, whereas devices made from P3HT and compound **1** only have responses up to about 650 nm. These spectral responses are consistent with the absorption spectra shown in Figure 1. However, the peak response of the device based on copolymer **4** is much lower than that of P3HT in the region of 300−600 nm and comparable to that of compound **1**.

Table 1. Characteristics of OSCs Based on Different Donor Materials Blended with PCBM

donor material	V_{OC} (V)	J_{SC} (mA cm^{-2})	FF	PCE (%)
copolymer **4**	0.61 ± 0.01	5.91 ± 0.08	0.57 ± 0.01	2.07 ± 0.04
P3HT	0.56 ± 0.01	7.60 ± 0.10	0.53 ± 0.01	2.28 ± 0.08
P3HT[a]	0.49 ± 0.01	9.87 ± 0.28	0.66 ± 0.01	3.22 ± 0.11
compound **1**	0.65 ± 0.01	3.49 ± 0.29	0.59 ± 0.03	1.34 ± 0.12

[a] Devices were fabricated under optimized conditions where the solvent was *o*-dichlorobenzene and the annealing temperature was 150 °C.

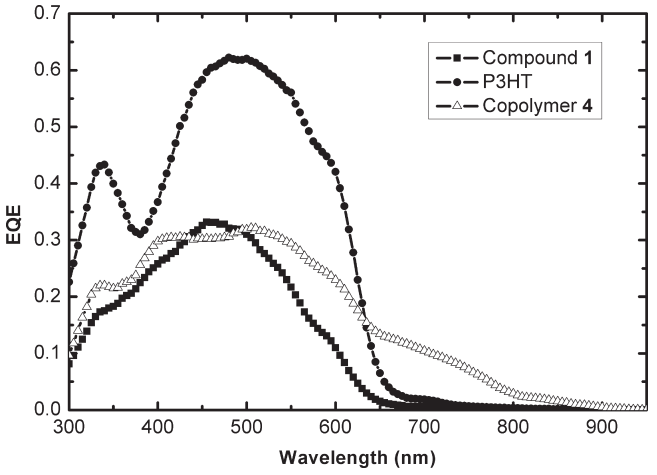

Figure 7. EQE spectra of the photovoltaic devices based on compound **1**, P3HT, and copolymer **4**.

The polymer characterizations show that copolymer **4** retains some of the crystallinity of P3HT, resulting in the relatively high FF of the device.[2] The higher performance of the device based on copolymer **4** compared with oligomer **1** is mainly due to the extended photocurrent response up to about 900 nm, which is the result of ICT between DPP unit and surrounding thiophene rings. However, the device performance of copolymer **4**, especially J_{SC}, did not exceed that of the P3HT device. This could be mainly attributed to the lower EQE of copolymer **4** in the region of 300−600 nm. The relatively low M_n of copolymer **4** could be responsible for this lower response, since the M_n of the polymer has been shown to influence its photovoltaic performance greatly.[37,38] It has also been reported that for DPP-based OSC devices polymers having lower M_n (10 000) drastically reduced the photocurrent compared with those having higher M_n (54 000), even if the devices were processed under identical conditions, possibly because of morphological changes.[16]

AFM was used to investigate the mixing morphology of the blend films. As shown in Figure 8a, the blend film of the oligomer:PCBM consists of clear fiber-like aggregations of compound **1**, while those of the polymers have uniform and featureless morphology as in Figures 8b and 8c. This difference could be because of the different molecular mobilities, which depend on M_n, since a large phase separation is often observed in low-M_n systems.[38,39] In contrast, the morphology of films based on copolymer **4** is similar to that of P3HT, indicating that the M_n of copolymer **4** is high enough to induce a uniform mixing morphology. The AFM images indicate that the relatively low M_n of copolymer **4** does not induce significant morphological change and therefore might not be responsible for the lower EQE response.

It has been previously shown that the EQE responses of OSC devices based on DPP-based polymers and PCBM are usually less than 50% and not as high as those of devices based on P3HT:PCBM.[9,16,40] The reason for this is still unclear at this stage; however, it is possible that the noncollinear structure of the segments on each side of the DPP unit weakens the conjugation along the main chain. This can be observed from the absorption peak in Figure 1. The absorption peak maximum of the copolymer **4** film is at 549 nm, which is smaller than that of the P3HT film (558 nm),

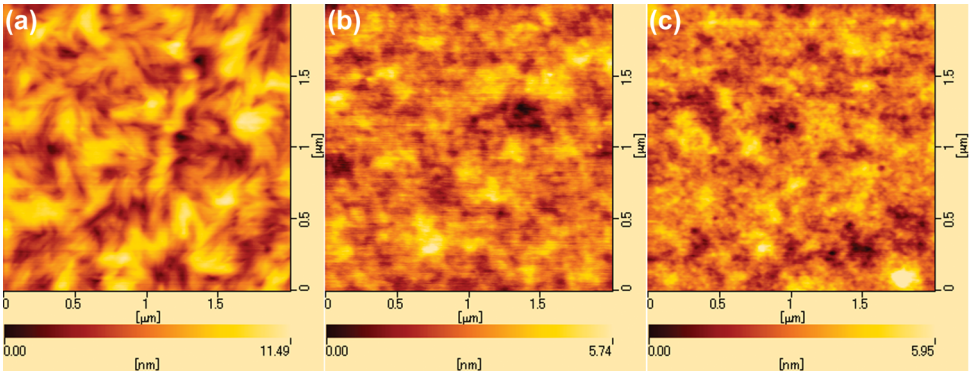

Figure 8. AFM height images in the tapping mode of the active layers blended with PCBM: (a) compound **1**, (b) P3HT, and (c) copolymer **4**.

dx.doi.org/10.1021/ma200287a |*Macromolecules* 2011, 44, 4222–4229

suggesting that the conjugation length becomes shorter after the introduction of the DPP unit. Kinks and torsion along the conjugated polymer main chain are usually considered as defects;[41] thus, the noncollinear structure of copolymer **4** may lead to charge recombination and/or charge leakage, resulting in lower EQE. Meanwhile, defects in the structure may also have an effect on the charge transport in the direction of the $\pi-\pi$ stacking. Although the incorporation of the DPP unit may enhance the $\pi-\pi$ stacking of the copolymers and decrease the interchain stacking distance, the noncollinearity could introduce defects into the copolymer, since some of the thiophene units in the backbone may lose their corresponding stacking units in the neighboring main chain. This could be the reason for the lower crystallinity and the reduced hole mobility of copolymer **4** when compared with commercial P3HT, and the EQE could be further decreased as a result. The choice of suitable acceptor units may furnish the copolymer with fewer defects and higher hole mobility, leading to better photovoltaic performance.

CONCLUSION

To achieve high mobility and broad light absorption required for OSCs, a new type of LBG copolymer was designed with a P3HT structure doped with electron-accepting units. The copolymer was synthesized by Stille coupling between the O3HT and the DPP unit. Direct stannylation was successfully performed on O3HT for the first time, despite its high and polydispersive molecular weight and two different end groups, providing a method of postfunctionalizing polythiophenes. The bandgap and energy levels of the resultant copolymer indicate that our design is a promising approach to enhancing OSC performance. We are currently investigating the effect of the molecular weights of the O3HT block and the copolymer as well as the choice of acceptor unit on the device performance.

ASSOCIATED CONTENT

Supporting Information. MALDI-TOF-MS and NMR spectra. This material is available free of charge via the Internet at http://pubs.acs.org.

AUTHOR INFORMATION

Corresponding Author

*E-mail: k-tajima@light.t.u-tokyo.ac.jp (K.T.); hashimoto@light.t.u-tokyo.ac.jp (K.H.).

ACKNOWLEDGMENT

The authors thank Dr. Chunhe Yang and Dr. Erjun Zhou for helpful advice on synthesis and characterization. This work was supported in part by the Global COE Program (Chemistry Innovation through Cooperation of Science and Engineering), MEXT, Japan. L.Z. thanks the Ministry of China for financial support under the Japanese Government (MONBUKAGAKUSHO: MEXT) Scholarship (Research Student).

REFERENCES

(1) Park, B.; Huh, Y. H.; Kim, M. *J. Mater. Chem.* **2010**, *20*, 10862.
(2) Kim, Y.; Cook, S.; Tuladhar, S. M.; Choulis, S. A.; Nelson, J.; Durrant, J. R.; Bradley, D. D. C.; Giles, M.; McCulloch, I.; Ha, C. S.; Ree, M. *Nature Mater.* **2006**, *5*, 197.
(3) Campoy-Quiles, M.; Ferenczi, T.; Agostinelli, T.; Etchegoin, P. G.; Kim, Y.; Anthopoulos, T. D.; Stavrinou, P. N.; Bradley, D. D. C.; Nelson, J. *Nature Mater.* **2008**, *7*, 158.
(4) Park, S. H.; Roy, A.; Beaupre, S.; Cho, S.; Coates, N.; Moon, J. S.; Moses, D.; Leclerc, M.; Lee, K.; Heeger, A. J. *Nature Photonics* **2009**, *3*, 297.
(5) Chen, Y. C.; Yu, C. Y.; Fan, Y. L.; Hung, L. I.; Chen, C. P.; Ting, C. *Chem. Commun.* **2010**, *46*, 6503.
(6) Wang, E.; Hou, L.; Wang, Z.; Hellström, S.; Zhang, F.; Inganäs, O.; Andersson, M. R. *Adv. Mater.* **2010**, *22*, 5240.
(7) Zhou, H. X.; Yang, L. Q.; Price, S. C.; Knight, K. J.; You, W. *Angew. Chem., Int. Ed.* **2010**, *49*, 7992.
(8) Wienk, M. M.; Turbiez, M.; Gilot, J.; Janssen, R. A. J. *Adv. Mater.* **2008**, *20*, 2556.
(9) Huo, L. J.; Hou, J. H.; Chen, H. Y.; Zhang, S. Q.; Jiang, Y.; Chen, T. L.; Yang, Y. *Macromolecules* **2009**, *42*, 6564.
(10) Hou, J. H.; Chen, H. Y.; Zhang, S. Q.; Li, G.; Yang, Y. *J. Am. Chem. Soc.* **2008**, *130*, 16144.
(11) Chen, C. H.; Hsieh, C. H.; Dubosc, M.; Cheng, Y. J.; Su, C. S. *Macromolecules* **2010**, *43*, 697.
(12) Yokoyama, A.; Miyakoshi, R.; Yokozawa, T. *Macromolecules* **2004**, *37*, 1169.
(13) Loewe, R. S.; Khersonsky, S. M.; McCullough, R. D. *Adv. Mater.* **1999**, *11*, 250.
(14) Sonar, P.; Singh, S. P.; Li, Y.; Soh, M. S.; Dodabalapur, A. *Adv. Mater.* **2010**, *22*, 5409.
(15) Woo, C. H.; Beaujuge, P. M.; Holcombe, T. W.; Lee, O. P.; Frechet, J. M. J. *J. Am. Chem. Soc.* **2010**, *132*, 15547.
(16) Bijleveld, J. C.; Zoombelt, A. P.; Mathijssen, S. G. J.; Wienk, M. M.; Turbiez, M.; de Leeuw, D. M.; Janssen, R. A. J. *J. Am. Chem. Soc.* **2009**, *131*, 16616.
(17) Tamayo, A. B.; Walker, B.; Nguyen, T. Q. *J. Phys. Chem. C* **2008**, *112*, 11545.
(18) Liang, F.; Lu, J.; Ding, J.; Movileanu, R.; Tao, Y. *Macromolecules* **2009**, *42*, 6107.
(19) Yue, W.; Zhao, Y.; Tian, H. K.; Song, D.; Xie, Z. Y.; Yan, D. H.; Geng, Y. H.; Wang, F. S. *Macromolecules* **2009**, *42*, 6510.
(20) Liang, Y. Y.; Xiao, S. Q.; Feng, D. Q.; Yu, L. P. *J. Phys. Chem. C* **2008**, *112*, 7866.
(21) Liang, V. Y.; Feng, D. Q.; Guo, J. C.; Szarko, J. M.; Ray, C.; Chen, L. X.; Yu, L. P. *Macromolecules* **2009**, *42*, 1091.
(22) Zhou, E. J.; Yamakawa, S. P.; Tajima, K.; Yang, C. H.; Hashimoto, K. *Chem. Mater.* **2009**, *21*, 4055.
(23) Zhang, Y.; Tajima, K.; Hirota, K.; Hashimoto, K. *J. Am. Chem. Soc.* **2008**, *130*, 7812.
(24) Miyakoshi, R.; Yokoyama, A.; Yokozawa, T. *J. Am. Chem. Soc.* **2005**, *127*, 17542.
(25) Wei, Q. S.; Miyanishi, S.; Tajima, K.; Hashimoto, K. *ACS Appl. Mater. Interfaces* **2009**, *1*, 2660.
(26) Iovu, M. C.; Sheina, E. E.; Gil, R. R.; McCullough, R. D. *Macromolecules* **2005**, *38*, 8649.
(27) Liu, J. S.; Loewe, R. S.; McCullough, R. D. *Macromolecules* **1999**, *32*, 5777.
(28) Lohwasser, R. H.; Bandara, J.; Thelakkat, M. *J. Mater. Chem.* **2009**, *19*, 4126.
(29) Gessner, V. H.; Daschlein, C.; Strohmann, C. *Chem.—Eur. J.* **2009**, *15*, 3320.
(30) Natori, I. *Macromol. Chem. Phys.* **2006**, *207*, 2215.
(31) Brown, P. J.; Thomas, D. S.; Kohler, A.; Wilson, J. S.; Kim, J. S.; Ramsdale, C. M.; Sirringhaus, H.; Friend, R. H. *Phys. Rev. B* **2003**, *67*, 064203.
(32) Scharber, M. C.; Wuhlbacher, D.; Koppe, M.; Denk, P.; Waldauf, C.; Heeger, A. J.; Brabec, C. L. *Adv. Mater.* **2006**, *18*, 789.
(33) Lee, J. U.; Jung, J. W.; Emrick, T.; Russell, T. P.; Jo, W. H. *J. Mater. Chem.* **2010**, *20*, 3287.
(34) Malik, S.; Nandi, A. K. *J. Polym. Sci., Part B: Polym. Phys.* **2002**, *40*, 2073.
(35) Salleo, A.; Kline, R. J.; DeLongchamp, D. M.; Chabinyc, M. L. *Adv. Mater.* **2010**, *22*, 3812.

(36) Zhang, Y.; Tajima, K.; Hashimoto, K. *Synth. Met.* **2011**, *161*, 225.
(37) Schilinsky, P.; Asawapirom, U.; Scherf, U.; Biele, M.; Brabec, C. J. *Chem. Mater.* **2005**, *17*, 2175.
(38) Ma, W.; Kim, J. Y.; Lee, K.; Heeger, A. J. *Macromol. Rapid Commun.* **2007**, *28*, 1776.
(39) Kline, R. J.; McGehee, M. D.; Kadnikova, E. N.; Liu, J. S.; Frechet, J. M. J. *Adv. Mater.* **2003**, *15*, 1519.
(40) Aich, R. B.; Zou, Y. P.; Leclerc, M.; Tao, Y. *Org. Electron.* **2010**, *11*, 1053.
(41) Kim, M. S.; Kim, B. G.; Kim, J. *ACS Appl. Mater. Interfaces* **2009**, *1*, 1264.